


Tryptophan-galactosylamine conjugates inhibit and disaggregate amyloid fibrils of A β 42 and hIAPP peptides while reducing their toxicity

Ashim Paul ¹, Moran Frenkel-Pinter ¹, Daniela Escobar Alvarez¹, Giulia Milordini², Ehud Gazit ¹,
Elsa Zacco ^{2,3}  & Daniel Segal^{1,4} 

Self-assembly of proteins into amyloid fibrils is a hallmark of various diseases, including Alzheimer's disease (AD) and Type-2 diabetes Mellitus (T2DM). Aggregation of specific peptides, like A β 42 in AD and hIAPP in T2DM, causes cellular dysfunction resulting in the respective pathology. While these amyloidogenic proteins lack sequence homology, they all contain aromatic amino acids in their hydrophobic core that play a major role in their self-assembly. Targeting these aromatic residues by small molecules may be an attractive approach for inhibiting amyloid aggregation. Here, various biochemical and biophysical techniques revealed that a panel of tryptophan-galactosylamine conjugates significantly inhibit fibril formation of A β 42 and hIAPP, and disassemble their pre-formed fibrils in a dose-dependent manner. They are also not toxic to mammalian cells and can reduce the cytotoxicity induced by A β 42 and hIAPP aggregates. These tryptophan-galactosylamine conjugates can therefore serve as a scaffold for the development of therapeutics towards AD and T2DM.

¹Department of Molecular Microbiology and Biotechnology, School of Molecular Cell Biology and Biotechnology, Tel Aviv University, Ramat Aviv, Tel Aviv 6997801, Israel. ²The Maurice Wohl Clinical Neuroscience Institute, King's College London, Brixton, London SE5 9RT, UK. ³RNA Central Lab, Center for Human Technologies, Istituto Italiano di Tecnologia, 16152 Genova, Italy. ⁴Sagol Interdisciplinary School of Neuroscience, Tel Aviv University, Ramat Aviv, Tel Aviv 6997801, Israel. email: elsa.zacco@iit.it; dsegal@post.tau.ac.il

A aberrant protein folding and consequent protein aggregation are hallmarks of a group of pathological conditions termed proteinopathies^{1,2}. Despite arising from different genetic, environmental and regulatory factors, most proteinopathies exhibit sub-cellular and molecular similarities, characterized by the accumulation of misfolded proteins that often, self-assemble into thermodynamically highly stable amyloid fibrils, which are resistant to proteolytic degradation and lack functionally stable amyloid fibrils^{3–7}.

Alzheimer's disease (AD) and type 2 diabetes mellitus (T2DM) are prime examples of proteinopathies^{2,6}. AD is the most common form of dementia in ageing populations^{8,9}. A major triggering neuropathological cause of AD is the misfolding and accumulation of A β 42, a hydrophobic peptide of 42-amino acids that is prone to self-assemble in the brain into toxic extra-cellular amyloid fibrils termed senile plaques^{9,10}. Protein self-assembly is also a key feature in T2DM¹¹. In this disease, pathological deposits of the peptide amylin, also called hIAPP, are found in the pancreatic islets of Langerhans of T2DM patients^{11,12}. hIAPP is a 37-amino acid neuroendocrine peptide hormone produced by β -cells together with insulin^{13,14}. When high insulin is required, such as in insulin deficiency, expression of hIAPP significantly increases, enhancing its propensity to aggregate into cytotoxic amyloid assemblies resulting in loss of β -cells and β -cell mass^{14,15}.

Epidemiological studies indicate comorbidity of AD and T2DM^{16,17}. Hyperglycemia increases the chance of developing AD by at least 2-fold by contributing to the accumulation of amyloid plaques on brain lesions^{16,18}. AD brains are less capable of glucose uptake from the surroundings, resembling a condition of insulin resistance¹⁹. In both T2DM and AD, oxidative stress is exacerbated, mitochondrial functions are impaired and neuron integrity compromised^{20–23}.

Intervening with the initial steps of protein misfolding and aggregation can thus be both a prophylactic measure and a means for modifying the course of these diseases^{24,25}. In both A β 42 and IAPP, the minimal aggregating sequence is a core of hydrophobic amino acids containing aromatic residues, KLVFFA and NFGAIL, respectively^{26–28}. Aromatic amino acids have been identified as crucial in the formation of various amyloid structures. π - π stacking, rather than mere hydrophobicity, was shown to provide energy, order and directionality to promote amyloid assembly^{29–31}. Based on these insights, peptide-based inhibitors were designed to contain aromatic residues whose side chains can intercalate the target amyloid aggregate and partially replace the original amino acids in π - π stacking^{32–36}. Along the same lines, small aromatic molecules, e.g. polyphenols, have been amply studied as inhibitors of amyloid aggregation, where the aromatic ring appears to similarly interfere with amyloid self-assembly^{37–41}.

Combining the aromatic elements of amino acids and small molecules has also been attempted for amyloid inhibition. For example, a naphthoquinone–tryptophan hybrid was shown to be effective towards various amyloids (including A β 42, IAPP, Tau, α -Syn) in vitro as well as in vivo^{42–46}. However, a major limitation in the drugability of such molecules is their poor solubility in aqueous media^{47–49}. Attaching a hydrophilic moiety for increasing solubility may enhance the overall therapeutic capacity of a drug⁴⁸. Functionalization with glycans has been proven to enhance solubility, half-life and specificity of certain drugs in vivo⁵⁰. The conjugation of glycans to peptides increases the overall interaction surface of the hybrid molecules, therefore increasing solubility by expanding the number of possible interactions with the solvent^{50–53}. Along the same rationale, aromatic molecules, which display high potential as anti-amyloidogenic agents, but are by themselves hydrophobic, were conjugated to mannitol and glucosamine^{43,54}.

Here we examined this concept by synthesizing tryptophan-galactosylamine hybrid molecules and tested their ability to inhibit the aggregation of A β 42 and hIAPP. Tryptophan was shown to be highly effective in intercalating the fibrils of various amyloidogenic proteins for inhibiting their aggregations^{42,44,45,55,56}. Galactose (Gal), one of the most abundant monosaccharide in the human body, plays a vital role in numerous biological processes, modulating and mediating them^{57,58}. To be able to speculate on the mechanistic role of galactose, we have included in the study GalNH₂ and GalNAc modifications at C2 of galactose influencing its charge density.

By means of Thioflavin T (ThT)-binding assay, circular dichroism (CD) spectroscopy, transmission electron microscopy (TEM) and Congo red birefringence, we show that the presence of galactose is key for the improved efficiency of tryptophan as amyloid inhibitor. The tested compounds are not toxic to mammalian cell lines. These results suggest that tryptophan-monosaccharide may be developed as disease-modifying therapeutics to target simultaneously A β 42 and hIAPP.

Results

Inhibition of A β 42 and hIAPP aggregation by hybrid molecules. To examine the possibility of combining an amino acid and a glycan into a potentially improved amyloid inhibitor, we conjugated tryptophan to the N-glycoside 1-amino-1-deoxy- β -D-galactose (galactosylamine) and to its variants derived from the substitution of the OH on C2 with NH₂ and NAc groups. For simplicity, the hybrid molecules resulting from the conjugation of tryptophan and these sugars are hereafter referred to as WGal, WGalNH₂ and WGalNAc. As a negative control, the dipeptide formed by two tryptophan, WW was included. The structure of these hybrids is shown in Fig. 1.

a A β 42 DAEFRHDSGYEVHHQKLVFFAEDVGSNKGAIIGLMVGGVVIA

b hIAPP KCNTATCATQRLANFLVHSSNFGAILSSTNVGSNTY

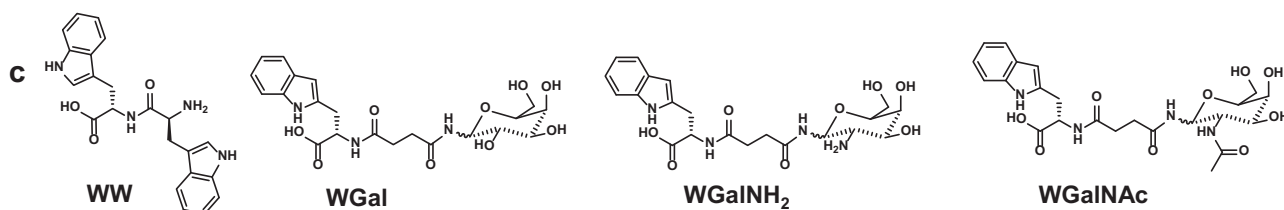


Fig. 1 Amyloidogenic peptides and aggregation inhibitors used in this study. **a** Amino acid sequence of A β 42. **b** Amino acid sequence of human hIAPP. **c** Structure of the dipeptide WW and of the tryptophan-galactosylamine hybrids WGal, WGalNH₂, and WGalNAc.

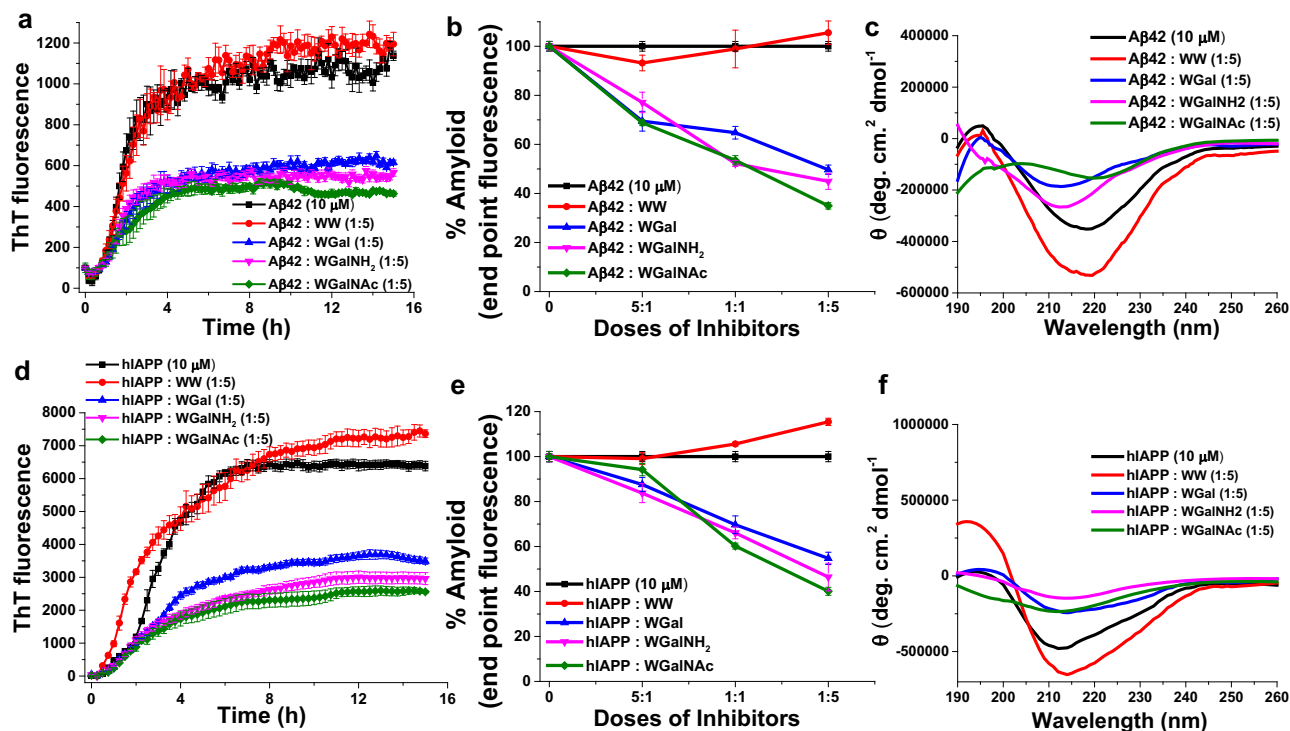


Fig. 2 Inhibition of amyloid formation of A β 42 and hIAPP by the tryptophan-galactosylamine hybrid molecules. **a** ThT kinetics of A β 42 aggregation in the absence or presence of 5-fold molar excess of the tested molecules. **b** Dose-dependent inhibition of A β 42 aggregation by the tested molecules. **c** CD analysis of conformational changes of the A β 42 aggregates in the absence or presence of the tested molecules. **d** ThT kinetics of hIAPP aggregation in the absence or presence of 5-fold molar excess of the tested molecules. **e** Dose-dependent inhibition of hIAPP aggregation by the tested molecules. **f** CD analysis of conformational changes of the hIAPP aggregates in the absence or presence of the tested molecules.

ThT was employed as an amyloid reporter dye to evaluate the effect of the tryptophan-galactosylamine hybrid molecules on amyloid formation by A β 42 and hIAPP (Fig. 2). ThT is known to intercalate within the amyloid fibrils resulting in fluorescence emission proportionate to the amyloid growth. Under our experimental conditions (pH 7.4 and 37°C), A β 42 (10 μ M) aggregation presented a sigmoidal curve, in agreement with previous studies^{59,60}. The curve reached a plateau after ca. 8 h, indicating the completion of amyloid fibril formation. Next, A β 42 was co-incubated with increasing doses of the tested hybrid molecules at peptide:hybrid molar ratios of 5:1, 1:1 and 1:5 (Fig. 2a, b and Supplementary Fig. 1). Considering the untreated A β 42 plateau value as 100% aggregation, in the presence of 5-fold molar excess of WGal, WGalNH₂ and WGalNAc the level of amyloid fibrils was reduced by ~50%, ~57%, and ~70%, respectively (Fig. 2a, b). Inhibition of A β 42 fibril formation by the hybrids was dose-dependent (Supplementary Fig. 1). WGalNAc was the statistically most effective among the inhibitors (Supplementary Fig. 2a). In contrast, no inhibition effect was recorded for the dipeptide control WW and for isolated galactosylamine and tryptophan at any A β 42:WW molar ratio (Fig. 2a, b and Supplementary Fig. 1a, e, f).

A similar inhibitory effect by the hybrid molecules was found toward hIAPP aggregation. In ThT kinetics, hIAPP was found to aggregate rapidly and reached plateau within ~6 h (Fig. 2d), indicating completion of amyloid fibrils formation in agreement with previous report⁴⁴. Upon co-incubation of hIAPP with the hybrid molecules, a dose-response inhibition of hIAPP fibril formation was observed (Fig. 2d, e and Supplementary Fig. 3). Maximum inhibition of ~45%, ~52%, and ~64% by WGal, WGalNH₂ and WGalNAc, respectively, was recorded at 5-fold molar excess of the hybrid molecules (Fig. 2d, e and

Supplementary Fig. 3). Also, for IAPP, the marginally stronger inhibitory effect of WGalNAc was statistically significant (Supplementary Fig. 2b). No inhibitory effect was recorded in the presence of the controls WW, isolated galactosylamine and tryptophan (Fig. 2d, e and Supplementary Fig. 3a, e, f).

CD spectroscopy in the absence or presence of increasing doses of the hybrid molecules was carried out for A β 42 and hIAPP to evaluate the effect of the conjugates on their conformation^{44,61} (Fig. 2c, f and Supplementary Figs. 4, 5). Aggregated A β 42 displayed a typical CD spectrum of β -sheet conformation with a single minimum at ~218 nm and a less intense maximum at around ~195 nm (Fig. 2c) as reported^{62–66}. This indicated that upon aggregation the peptide transitioned from an initial disordered random coil structure to a highly organized β -rich conformation. The presence of the tested molecules during A β 42 aggregation at a peptide:hybrid molar ratio of 5:1 did not alter the CD profile (Supplementary Fig. 4). However, the addition of equimolar amounts of WGal determined a diminished intensity minimum in the A β 42 CD profile and a shifted band from 218 nm to 212 nm (Supplementary Fig. 4b). This effect was more pronounced at 5-fold molar excess of WGal, under which condition, the CD intensity was reduced markedly and the peak shifted from 218 nm to 211 nm (Fig. 2c), indicating a substantial reduction of β -sheet content as observed for other amyloid inhibitors of A β 42^{44,65,66}. A similar effect on the secondary structure of A β 42 was observed in the presence of WGalNH₂ and WGalNAc (Fig. 2c and Supplementary Fig. 4c, d). No significant variation on the A β 42 secondary structure was observed in the presence of the control WW (Fig. 2c and Supplementary Fig. 4a).

CD analysis was performed also for hIAPP (Fig. 2f and Supplementary Fig. 5). Aggregated hIAPP fibrils showed a positive peak at ~195 nm and a negative peak at ~213 nm,

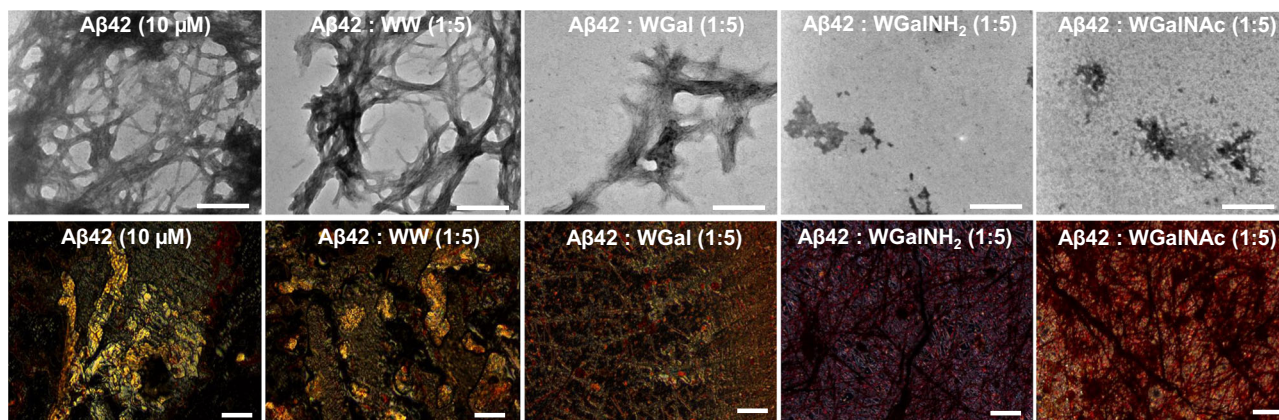


Fig. 3 Analysis of A β 42 fibrils in the absence or presence of the tryptophan-galactosylamine hybrid molecules. TEM (upper panel) and Congo red stained birefringence (bottom panel) images of A β 42 fibrils in the absence or presence of 5-fold molar excess of the tested molecules. Scale bars: 200 nm in TEM micrographs and 100 nm in Congo red birefringence images.

suggesting a β -sheet-rich conformation in agreement with previous reports^{33,44,67,68}. With different degrees of effectiveness, the presence of all tested hybrid molecules caused a reduction of the intensity of the CD signal, indicating an overall lower of β -sheet content of hIAPP (Fig. 2f and Supplementary Fig. 5). WGalNH₂ and WGalNAc had a slightly more pronounced effect on the secondary structure of hIAPP compared to WGal (Fig. 2f and Supplementary Fig. 5). In the case of hIAPP, a substantial effect was also recorded by the control WW (Fig. 2f and Supplementary Fig. 5a): increasing doses of WW resulted in a proportionate increment of the intensity of the maximum at 195 nm and a slight increase of the intensity of the minimum, accompanied by a minor shift towards higher wavelengths, from 212 to 220 nm.

Next, we evaluated the effect of the hybrid molecules on the morphology and abundance of A β 42 and hIAPP fibrils by means of TEM and Congo red birefringence^{69–71}. In the absence of the hybrid molecules, A β 42 formed long fibrils organized in characteristic packed bundles of different thickness, clearly visible in TEM micrographs (Fig. 3, upper panel)^{44,72,73}. These fibrils also generated the amyloid specific gold-green birefringence upon staining with Congo red (Fig. 3, bottom panel and Supplementary Fig. 6)⁷⁴. In the presence of 5-fold excess of WGalNH₂ or WGalNAc no fibrillar morphology was observed but small, amorphous aggregates appeared, indicating that these two hybrids significantly inhibited A β 42 amyloid formation. In the presence of WGal, A β 42 fibrillar morphology was still distinguishable, albeit the fibers were considerably fewer and smaller, indicating that this molecule was able to reduce the amount and the size of assemblies. In contrast, the control WW did not display any effect on the morphology of the A β 42 amyloid fibrils at the same molar ratio (Fig. 3, upper panel). Similarly, no Congo red gold-green birefringence was observed when A β 42 was incubated with WGalNH₂ or WGalNAc. In the presence of WGal we detected traces of birefringence, albeit minor, whereas intense gold-green birefringence was observed in the presence of the control molecule WW, indicating that it did not inhibit A β 42 fibril formation (Fig. 3, bottom panel and Supplementary Fig. 6).

Similar analyses on hIAPP demonstrated that, in the absence of the hybrid molecules, hIAPP formed a thick network of amyloid fibrils, as shown by TEM (Fig. 4, upper panel), and exhibited golden birefringence upon staining with Congo red (Fig. 4, bottom panel and Supplementary Fig. 7) as reported^{33,44,67}. When hIAPP was incubated with 5-fold molar excess of the hybrid molecules, no typical fibrillar assemblies were observed, rather some amorphous aggregates of different sizes were

detected (Fig. 4, upper panel). Likewise, no birefringence was observed, indicating inhibition of amyloid formation. In contrast, in the presence of the control WW, hIAPP amyloid fibrils were clearly visible in a more densely packed network and a clear gold-green birefringence was detectable. These results may suggest that not only WW was unable to inhibit the aggregation of hIAPP, but also that this dipeptide may promote further aggregation of hIAPP.

Collectively, the ThT, CD and TEM studies indicated that the tryptophan-galactosylamine hybrids were efficient in inhibiting aggregation and amyloid fibril formation of both A β 42 and hIAPP. The control WW molecule lacked such inhibitory effect.

Hybrid molecules disaggregate pre-formed peptides' fibrils. For efficient treatment of proteinopathies it may be advantageous to disassemble amyloid aggregates/fibrils which are usually already present at the time of diagnosis^{75–77}. Therefore, the ability of the hybrid molecules to disrupt pre-formed fibrils of A β 42 and hIAPP was examined. To this end, A β 42 and hIAPP peptides were allowed to aggregate for 10 h in the absence of the hybrid molecules. According to the ThT kinetic results, this time was sufficient to complete fibril formation (Fig. 2a, d). Then, various doses of the hybrid molecules were added to the pre-formed fibrils and the mixtures were incubated for additional 10 h. The process of disaggregation was monitored by ThT-binding assay, CD spectroscopy, TEM and Congo red staining (Fig. 5).

ThT fluorescence intensity remained at a plateau when A β 42 was untreated, indicating that fibrils were maintained throughout the duration of the assay (Fig. 5a, b and Supplementary Fig. 8). Following addition of the hybrid molecules, the ThT signal dropped in a dose-dependent manner, reflecting a reduction in the amount of pre-formed fibrils (Fig. 5a, b and Supplementary Fig. 8). Maximum disruption, observed in the presence of 5-fold excess of the hybrid molecules, revealed ~40%, 52%, and 61% disaggregation in the presence of WGal, WGalNH₂, and WGalNAc, respectively (Fig. 5b and Supplementary Fig. 9a). In the presence of the control molecule WW, ThT fluorescence intensity was instead increased by ~20%, indicating that WW not only was unable to disaggregate the pre-formed fibrils, but also it may mediate the formation of new amyloid fibrils (Supplementary Fig. 9a). CD analysis (Fig. 5c and Supplementary Fig. 10) supported these findings. Untreated pre-formed A β 42 fibrils exhibited a negative peak at ~214 nm and a positive maximum at ~194 nm, indicating β -sheet-rich conformation, whereas the intensity at ~214 nm was reduced in a dose-dependent manner in the presence of the hybrid molecules,

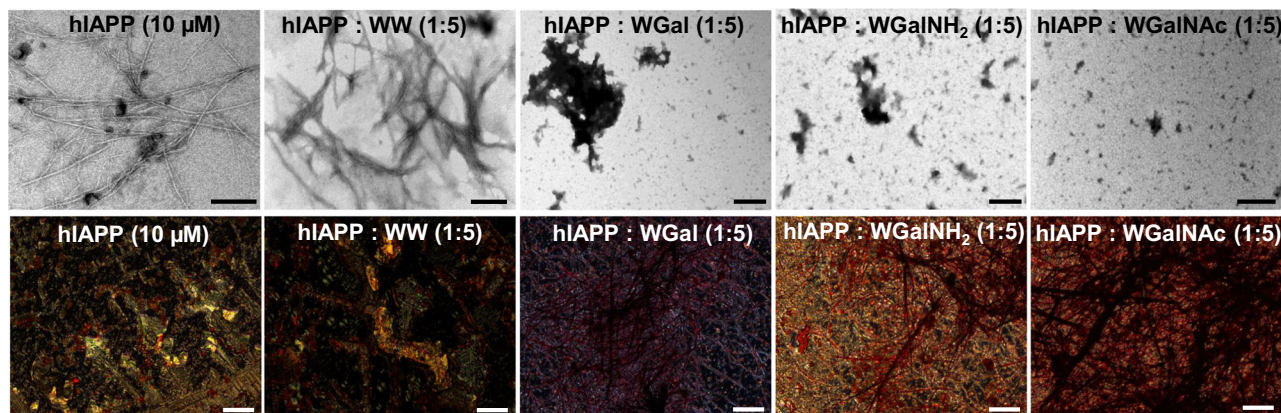


Fig. 4 Analysis of hIAPP fibrils in the absence or presence of the tryptophan-galactosylamine hybrid molecules. TEM (upper panel) and Congo red stained birefringence (bottom panel) images of hIAPP fibrils in the absence or presence of the 5-fold molar excess of the tested molecules. Scale bars: 200 nm in TEM micrographs and 100 nm in Congo red birefringence images.

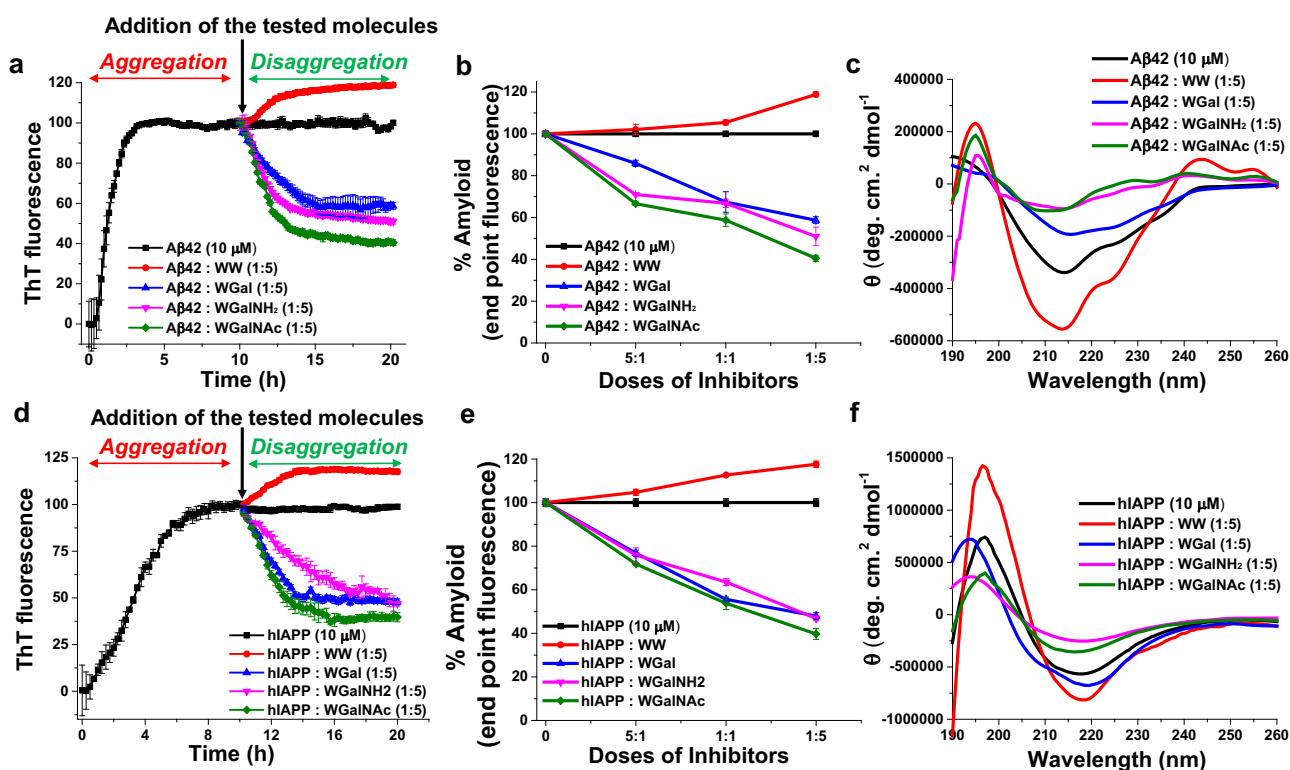


Fig. 5 Effect of the tryptophan-galactosylamine hybrid molecules on pre-formed fibrils of A β 42 and hIAPP. **a** ThT kinetics for the disaggregation of pre-formed fibrils of A β 42 in the absence or presence of 5-fold molar excess of the tested molecules. **b** Dose-dependent disaggregation of pre-formed fibrils of A β 42 by the tested molecules. **c** CD analysis of pre-formed A β 42 of in the absence or presence of the tested molecules. **d** ThT kinetics for the disaggregation of pre-formed fibrils of hIAPP in the absence or presence of 5-fold molar excess of the tested molecules. **e** Dose-dependent disaggregation of pre-formed fibrils of hIAPP by the tested molecules. **f** CD analysis of pre-formed hIAPP fibrils in the absence or presence of the tested molecules. Arrows in (**a**, **d**), indicate time of adding the tested hybrid molecules.

suggesting a substantial reduction in β -sheet content (Fig. 5c and Supplementary Fig. 10).

Comparable results were obtained for disaggregation of pre-formed hIAPP fibrils. (Fig. 5d, e and Supplementary Fig. 11). In the absence of the hybrid molecules, the ThT signal remains at a plateau, indicating that the presence of hIAPP fibrils in solutions during the assay (Fig. 5d, e and Supplementary Fig. 11). In contrast, in the presence of the hybrid molecules the ThT signal was reduced in a dose-dependent manner. Maximal reduction of signal, noticed at 5-fold excess of the hybrid molecules, represented ~53%, 53%, and 60% disaggregation in

the presence of WGal, WGalNH₂, and WGalNAc, respectively (Fig. 5e and Supplementary Fig. 9b). In contrast, a statistically significant 20% increase of ThT signal was observed in the presence of the control WW (Supplementary Fig. 9b). CD results corroborated these observations. Untreated pre-formed hIAPP fibrils exhibited a negative peak at ~217 nm and a maximum at ~196 nm, indicating β -sheet-rich conformation. In the presence of the hybrid molecules, the intensity at ~216 nm was reduced in a dose-dependent manner, suggesting a substantial reduction of β -sheet content (Fig. 5f and Supplementary Fig. 12).

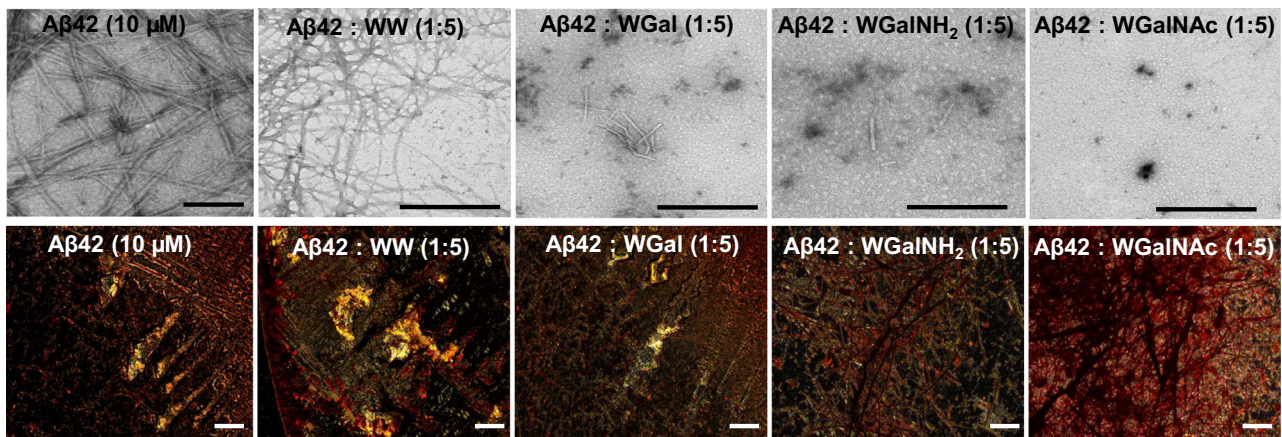


Fig. 6 Analysis of pre-formed A β 42 fibrils in the absence or presence of the tryptophan-galactosylamine hybrids. TEM (upper panel) and Congo red stained birefringence (bottom panel) images of A β 42 fibrils in the absence or presence of the 5-fold molar excess of the tested molecules. Scale bars: 200 nm in TEM micrographs and 100 nm in Congo red birefringence images.

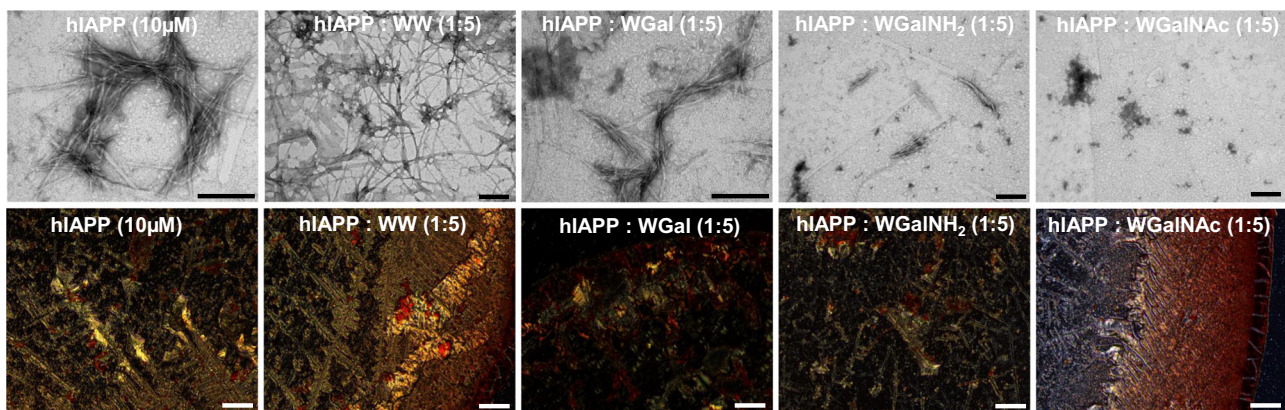


Fig. 7 Analysis of pre-formed hIAPP fibrils in the absence or presence of the tryptophan-galactosylamine hybrid molecules. TEM (upper panel) and Congo red stained birefringence (bottom panel) images of pre-formed hIAPP fibrils in the absence or presence of the 5-fold molar excess of the tested molecules. Scale bars: 200 nm in TEM micrographs and 100 nm in Congo red birefringence images.

TEM and Congo red assays lent further support to the ThT and CD results of the disaggregation experiments. Untreated pre-formed A β 42 assemblies exhibited a fibrillar network indicative of the presence of amyloids (Fig. 6). However, in the presence of 5-fold excess of all tested hybrid molecules the fibril density was reduced, but the magnitude of this effect was different for each compound. No trace of fibrils was detected in the presence of WGalNAc, indicating an apparent transformation of the pre-formed fibrils into amorphous structures. WGalNH₂ was somewhat less efficient and WGal even less so (Fig. 6, upper panel). Congo red staining showed gold-green birefringence in untreated pre-formed A β 42 fibrils (Fig. 6, bottom panel and Supplementary Fig. 13), yet no birefringence was observed when the pre-formed fibrils were incubated with WGalNH₂ or WGalNAc. However, in the presence of WGal or of the control WW faint birefringence was detected (Fig. 6, bottom panel and Supplementary Fig. 13).

Similar analyses of pre-formed hIAPP fibrils indicated that the untreated peptide exhibited dense fibrillar morphology and strong golden birefringence (Fig. 7); yet, upon treatment with WGal and WGalNH₂, the levels of amyloid fibrils and of Congo red birefringence were substantially reduced. No fibrils were detected by TEM in the presence of WGalNAc (Fig. 7, upper panel), and Congo red birefringence was markedly reduced, indicating complete disaggregation of pre-formed hIAPP fibrils (Fig. 7, bottom panel and Supplementary Fig. 14). In contrast, upon incubation with WW, fibril morphology and Congo red

birefringence were unchanged compared to the hIAPP peptide alone, suggesting that WW was unable to disaggregate the pre-formed fibrils of hIAPP (Fig. 7 and Supplementary Fig. 14).

Taken together, these results indicate an efficient disaggregation of the pre-formed assemblies of A β 42 and hIAPP by the three hybrid molecules, among which WGalNAc was found to be the most effective.

Hybrid molecules reduce A β 42 and hIAPP-induced toxicity.

The effect of the tryptophan-galactosylamine hybrid molecules toward cytotoxicity caused by A β 42 and hIAPP amyloids was evaluated. To this end, we first tested whether the hybrid molecules carried any cytotoxicity themselves. We incubated them at various concentrations (1–250 μ M) with either human neuroblastoma (SH-SY5Y) or with human embryonic kidney (HEK-293) cell lines and assessed cell viability by XTT assay^{33,44}. No considerable toxicity ($\geq 95\%$ viability) was caused by the hybrid molecules towards either cell line, even at the highest concentration of 250 μ M (Fig. 8). However, the control molecule WW exhibited a slightly toxic effect at this concentration, and $\sim 88\%$ and $\sim 83\%$ viability was observed for SH-SY5Y and HEK-293 cells, respectively.

To examine the effect of the hybrid compounds on the cytotoxicity caused by A β 42 and hIAPP aggregates towards these cell lines, A β 42 and hIAPP peptides were first incubated, separately, at various concentrations (1–20 μ M) to allow fibril

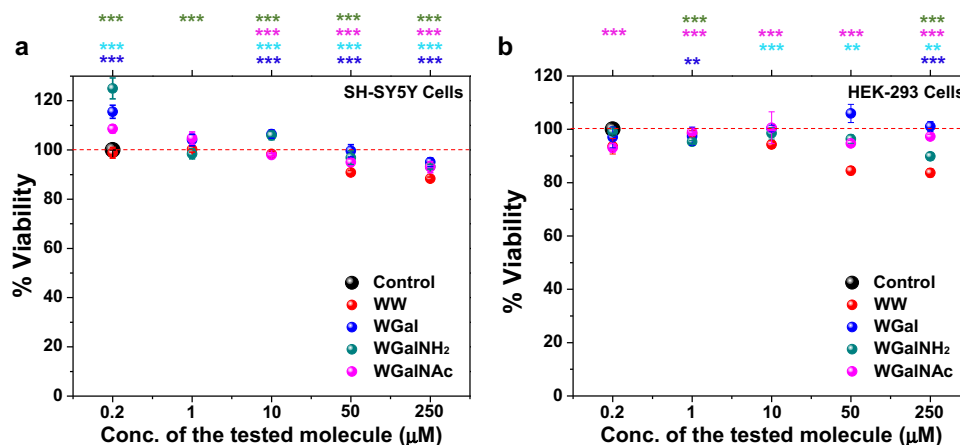


Fig. 8 Evaluation of cytotoxicity of the tryptophan-galactosylamine hybrid molecules. The toxicity of the hybrid molecules towards (a) SH-SY5Y and (b) HEK-293 cells evaluated by XTT assay. Cells were treated with various concentrations (1–250 μM) of the hybrid molecules and incubated for 24 h. ***p* < 0.005 and ****p* < 0.001 compared to untreated samples. Untreated cells were considered as 100% viable.

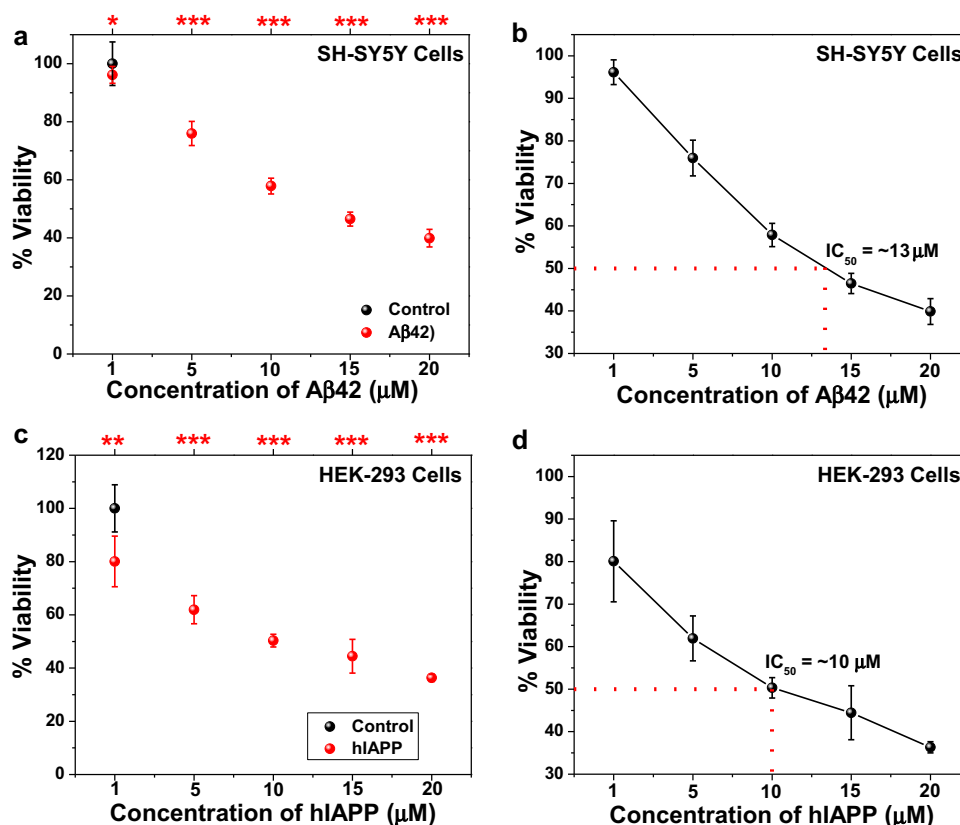


Fig. 9 Evaluation of IC₅₀ for Aβ42 and hIAPP aggregates. **a** Effects of pre-formed Aβ42 fibrils on viability of SH-SY5Y cells were examined using XTT reduction assay. **b** IC₅₀ value of Aβ42 assemblies was calculated from the XTT assay and found as ~13 μM. **c** Effects of pre-formed hIAPP fibrils on viability of HEK-293 cells were examined using XTT reduction assay. **d** IC₅₀ value of pre-formed hIAPP fibrils was calculated from the XTT assay and found as ~10 μM. Confluent cells were incubated with various concentrations (1–20 μM) of pre-formed Aβ42 and hIAPP fibrils (generated based on ThT results). After 24 h incubation with the peptides, cell viability was determined by XTT reduction assay. ***p* < 0.05, ***p* < 0.005 and ****p* < 0.001 compared to untreated cells. Untreated cells were considered as 100% viable.

formation. The peptide assemblies were then incubated for further 24 h with SH-SY5Y or HEK-293 cells and cell viability was monitored by XTT assay (Fig. 9). The calculated IC₅₀ values for Aβ42 and hIAPP were found to be ~13 μM and ~10 μM, respectively, as compared to untreated control cells, in agreement with previous reports^{44,78,79}. Various doses of

the hybrid molecules (Aβ42/hIAPP:hybrids = 50:1, 20:1, 10:1, 5:1, 1:1, 1:5, 1:10, 1:20) were added separately to pre-aggregated Aβ42 (13 μM) or hIAPP (10 μM). The mixtures were then independently applied to the respective cells for 24 h, and cell viability was further measured by XTT assay (Fig. 10a).

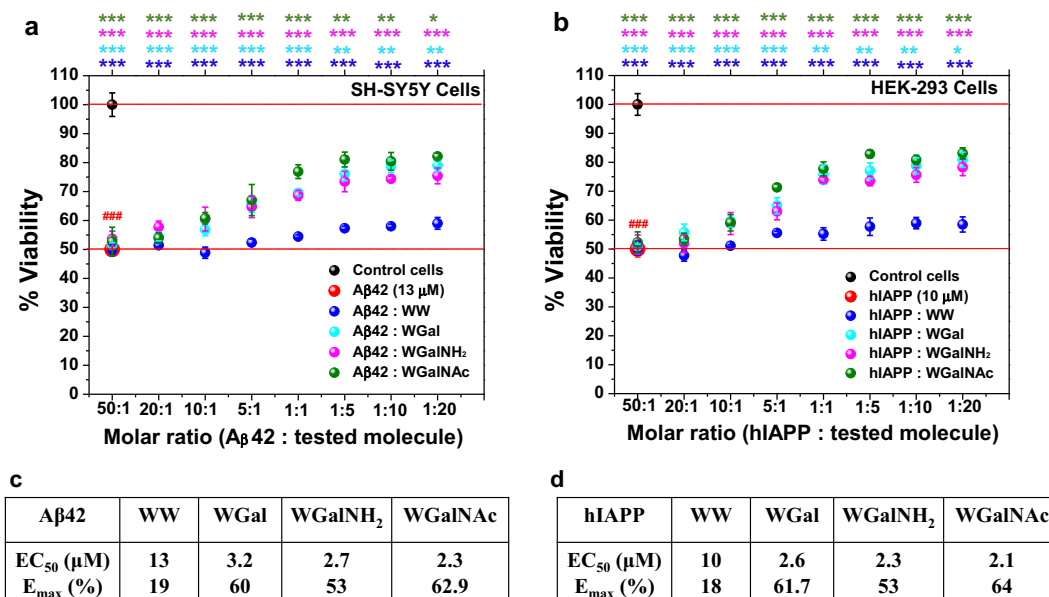


Fig. 10 Effects of the tryptophan-galactosylamine hybrid molecules towards cytotoxicity of pre-formed amyloids. (a) Aβ42- and (b) hIAPP-induced cytotoxicity in the presence or absence of various doses of the tested molecules were evaluated using XTT reduction assay. EC₅₀ and E_{max} of the tested molecules when applied to reduce the cytotoxicity induced by pre-formed fibrils of (c) Aβ42 and (d) hIAPP. ###*p* < 0.001, compared to the untreated cells. ***p* < 0.05, ***p* < 0.005 and ****p* < 0.001 compared to Aβ42 (a) and hIAPP (b) treatment. Untreated cells were considered as 100% viable.

All of the tested hybrid molecules, including the control WW, significantly reduced the toxicity of pre-formed Aβ42 fibrils in a dose-dependent manner. For example, 20-fold excess of WW, WGal, WGalNH₂ and WGalNAc caused an increase in viability of cells, incubated with pre-aggregated Aβ42, of 19%, 60 ± 4%, 53 ± 5%, and 62.9 ± 2%, respectively (maximum effect, or E_{max}) (Fig. 10a and Supplementary Fig. 15). In agreement with the in vitro assays, in the cell-based assays WGalNAc gave the highest effect, with an EC₅₀ of 2.3 μM. WW, WGal and WGalNH₂ resulted in EC₅₀ of 13, 3.2 and 2.7 μM, respectively (Fig. 10a, c and Supplementary Fig. 15a).

Similarly, when HEK-293 cells were exposed to pre-formed hIAPP fibrils, in the absence or presence of various doses of the hybrid molecules, cell viability was found to be increased proportionately to the dose of the hybrid molecules. 20-fold excess of WW, WGal, WGalNH₂ and WGalNAc incremented the viability of 18 ± 5%, 61.7 ± 5%, 53 ± 5%, and 64 ± 4% respectively (maximum effect, or E_{max}) (Fig. 10b, d and Supplementary Fig. 15b). The calculated EC₅₀ was 10, 2.6, 2.3, and 2.1 μM, respectively (Fig. 10b, d and Supplementary Fig. 15b).

These results indicated that the hybrid molecules significantly reduced the cytotoxic effect induced by Aβ42 and hIAPP fibrils. WGalNAc was the most effective among them.

Discussion

In this work, we evaluated the potential of a new class of highly-soluble tryptophan-galactosylamine hybrid molecules to alter the progression of the aberrant aggregation of the disease-associated peptides Aβ42 and hIAPP, both in vitro and in mammalian cell lines.

The amino acid tryptophan was chosen in this study because it was reported to display the most amyloidogenic propensity among the proteinogenic amino acids, suggesting a potentially strong involvement of its aromatic side chain in the molecular associations leading to the formation of amyloid fibrils^{55,80}. Indeed, tryptophan has been shown to be directly involved in the abrogation of protein aggregation by targeting the aromatic

recognition interfaces of amyloidogenic proteins⁴². Tryptophan derivatives have been employed in the design of several inhibitors of amyloid formation. For example, tryptophan-containing peptides have been employed to reduce Aβ42-derived toxicity in animal models⁸¹. Tryptophan-coated gold and silver nanoparticles have been shown to inhibit both spontaneous and seed-induced aggregation of insulin⁸². Naphthoquinone-tryptophan hybrids displayed promising potential for mitigating the amyloidogenicity of several proteins and peptides^{44,45,83}.

The present work aimed at improving the drugability of tryptophan by combining its ability to target amyloid species with a component that would confer the capacity to dissolve the target protein aggregates. Thus, we postulated that the conjugation of tryptophan to a glycan unit could increase solubility and target selectivity of the hybrid molecule^{50,84,85}.

The glycan galactose is involved in numerous biological processes, hence galactosylation is considered as a useful tool for delivery of therapeutics^{86–88}. For example, galactosylated nano-carriers have been shown to improve site-specific delivery of siRNA and anticancer drugs⁸⁶. Indeed, galactose has been employed in studies for the treatment and diagnosis of several diseases, as well as vaccine development^{89–91}. D-galactose, together with D-glucose, are actively transported across the blood-brain barrier (BBB), making these hexoses highly attractive for the specific delivery of drugs to the brain⁹². Galactose-conjugated dopamine was found to have better BBB permeability, bioavailability, and therapeutic effects against Parkinson's disease^{93–95}. Finally, galactose is a preferred glycan candidate for targeting hIAPP because, due to hepatic metabolism, insulin and glucose level responses to galactose are lower than for glucose^{96,97}.

Taken together, this evidence points to tryptophan and galactose as desirable building blocks for the design of potential hybrid molecules against amyloid formation.

At the core of the amyloidogenic process there are conformational changes of the native, soluble peptides into unstable oligomers that subsequently assemble into insoluble protofibrils and fibrils⁹⁸. The formation of oligomers in the absence of other pre-existent larger peptide species is referred to as primary

nucleation⁹⁹. These oligomers can grow into fibers by the addition of other oligomers (elongation) or monomers (secondary nucleation)⁶⁰. The kinetics of amyloid formation generally follows a sigmoidal trend, in which a stable lag phase, an exponential phase and a plateau, the stage by which no more monomers are available, can be distinguished^{100,101}. According to the mechanism of action of a potential inhibitor, any of the phases of the aggregation process may be affected. All our *in vitro* analyses demonstrated an appreciable amyloid inhibitory effect on both A β 42 and hIAPP by all the tryptophan-galactosylamine hybrids. The data collected for WGal, WGalNH₂ and GalNAc show that there is no kinetic effect caused by the inhibitors on primary nucleation or elongation (lag phase or exponential phase). Instead, the plateau levels of both A β 42 and hIAPP are significantly reduced by the presence of the hybrid molecules. To speculate on the mechanistic role that these inhibitors are playing on the aggregation of the target peptides, it is important to bear in mind that there are many ways by which small molecules may model the aggregation pathway^{102,103}. Among these, it has been reported that various inhibitors reduce the amount of amyloids by redirecting the aggregation towards alternative off-path products, rather than preventing the self-assembly of the monomers^{41,104–106}. We believe that this is the case for the hybrid molecules studies here: the lack of an obvious kinetic effect on primary/secondary nucleation or elongation suggests the sequestration of the monomers and oligomers to a parallel alternative pathway that does not lead to amyloid formation but to smaller and often amorphous assemblies. This hypothesis is supported by the ca. 50% reduction of ThT-positive aggregates in the presence of the inhibitors; by the variation in A β 42 and hIAPP's secondary structures; by the lack of fiber-like assemblies as shown by TEM and Congo red birefringence; and by the significant lower cellular toxicity.

A closer look into the results of the ThT-binding assays suggests that although the differences between the effects of the inhibitors are small, WGalNAc is on average a significantly stronger amyloid inhibitor compared to WGal and WGalNH₂, as indicated by the *p*-value calculations (Supplementary Figs. 2, 9). The superiority of WGalNAc may be accounted for by its acetyl group. This moiety may actively contribute to increase the energetically favorable CH- π stacking between the cluster of carbon atoms of the hexose ring and the target peptides^{107,108}. Moreover, the larger molecular radius of -NAc compared to -NH₂ and -OH may allow WGalNAc to interact more stably with a higher number of atoms of the target peptides¹⁰⁹. Finally, the slightly more hydrophobic acetyl group may also participate in binding the amyloidogenic peptides tested, and lead the whole hybrid molecule WGalNAc towards a more balanced equilibrium between the ideal hydrophilicity and hydrophobicity¹¹⁰.

Alongside the designed hybrid molecules, all experiments performed in this work included the dipeptide WW, here referred to as “negative control” which allowed to assert the effect of the galactosylamine derivatives in comparison to the tryptophan alone. However, in some circumstances, WW displayed a stimulatory effect on the aggregation of A β 42 and hIAPP. This behavior became more pronounced and statistically significant (Supplementary Figs. 2, 9) during the disaggregation of pre-formed fibrils (Figs. 5–7). These results could be explained by the amyloidogenic nature of tryptophan and by its ability to self-assemble into fibrils, resulting in an additive aggregation level^{55,80}. The co-presence of aggregating peptides may have functioned as further nucleation agent for the π - π stacking of tryptophan, which, on its end, could also have consequently induced further A β 42 and hIAPP aggregation into mature amyloid fibrils. This effect, however, did not translate into an increment of toxicity in the *in-cell* assays: albeit not as efficiently, WW,

like the hybrid molecules, reduced the cytotoxicity induced by extra-cellular pre-aggregated A β 42 and hIAPP. To explain the partial inhibitory effect of WW on A β 42 and hIAPP-induced toxicity, we postulate that WW may have driven the aggregates of these peptides towards larger bundle of fibrils, which are reported to be less toxic than smaller oligomeric forms^{111–114}. WW's effect on cytotoxicity, however statistically significant, is very weak when compared to the hybrid molecules: EC₅₀ of all hybrids are between 2.5 and 5-fold lower than the one calculated for WW.

Significant breakthroughs in inhibition of disease associated amyloid aggregation have led to different therapeutic strategies, which include targeting the protein of interest with either small molecules or antibodies^{115–117}. Despite the efforts and the sophisticated specificity offered by anti-aggregation antibodies, these have so far failed at clinical trials because of the aberrant immune response they initiate^{118,119}. In this sense, small molecules offer substantial advantages over antibodies, since they are immunologically tolerated, more stable in the cellular environment, and often offer higher potential of crossing the BBB¹²⁰.

In this work we presented anti-aggregating tryptophan-galactosylamine hybrid small molecules. We show a dual effect of these small molecules, capable of both reducing and reversing the formation of amyloid fibrils. Moreover, these molecules are non-toxic toward mammalian neuroblastoma and kidney cell lines and are able to significantly reduce the cytotoxicity induced by pre-formed fibrils of A β 42 or hIAPP. Collectively, the results here reported indicate that the hybrid system could be employed as a scaffold in the development of therapeutics towards multiple proteinopathies. Further studies will follow to obtain deeper insight on the mechanism of action of these hybrid molecules and to chemically improve them for higher efficacy and *in vivo* validation. Amyloids of A β 42 and hIAPP co-exist in major age-related diseases. Thus, the hybrid molecules could potentially offer single disease-treating therapeutics to these disorders.

Methods

Materials and sources. A β 42 was purchased from rPeptide (USA). hIAPP was purchased from Peptide 2.0 (USA). The inhibitors (WGal, WGalNH₂ and WGalNAc) were purchased from Aldlab (USA). WW was purchased from GL Biochem Shanghai (China). Lipids were purchased from Avanti Polar Lipids (USA). All chemicals and reagents were of analytical grade. Unless otherwise stated, all chemicals were obtained from Sigma-Aldrich (Rehovot, Israel).

Stock preparation. A β 42 and hIAPP were monomerized by a 10 min pre-treatment with HFIP and the solvent was evaporated using a Speed Vac. The resulting thin films were dissolved in PBS (100 mM, pH 7.4) and sonicated for 5 min to get a stock concentration of 50 μ M, which immediately diluted to required concentration for an experiment. Stock solutions of ThT (4 mM in PBS) and hybrid molecules (10 mM in PBS) were prepared. All the stock solutions were diluted according to the requirement.

Thioflavin T-binding assay. For the aggregation kinetics, the stock solutions of A β 42 or hIAPP were diluted in a 96-well black plate so that the final mixture (100 μ l) contained 10 μ M peptide and 20 μ M ThT in 100 mM PBS. The experiment was performed according to the previous report⁴⁴. For fibril disassembly assays, A β 42 and hIAPP were first allowed to self-assemble until a ThT-associated plateau was reached; the hybrid molecules were then added separately to designated wells (peptide: hybrid molecule = 5:1, 1:1, 1:5), and the fluorescence values were further followed until a new plateau was reached. Kinetics fluorescence data were collected at 37 °C in triplicate using Infinite M200 microplate reader (Tecan, Switzerland), with measurements acquired at 15 min intervals. Excitation and emission wavelengths were set at 440 nm and 485 nm, respectively.

Circular dichroism spectroscopy. To analyze the secondary structure of the aggregated or disassembled peptides, 300 μ l samples (10 μ M of A β 42 and hIAPP) were placed in a quartz cuvette (path length 1 mm) and CD spectra were recorded on a Chirascan spectrometer between 190–260 nm. The blank was subtracted from the acquired CD spectra. For the CD study in the presence of the tryptophan-galactosylamine molecules, the spectra of hybrid molecules were also recorded separately and subtracted from the respective sample spectra. The normalized data were plotted using Origin pro 2015 software.

Transmission electron microscopy. Samples (10 μ L) were placed for 2 min on 400-mesh copper grids covered with carbon-stabilized Formvar film (Electron Microscopy Sciences (EMS), Hatfield, PA). Excess fluid was removed, and grids were negatively stained with 2% uranyl acetate solution (10 μ L) for 2 min. After excess fluid removal, the samples were visualized using a JEM-1400 TEM (JEOL), operated at 80 kV.

Cell cytotoxicity experiments. The SH-SY5Y and HEK-293 cell lines (2×10^5 cells/mL) were cultured in 96-well tissue microplates (100 μ L/well) and allowed to adhere overnight at 37 °C. The conjugate molecules were dissolved in DMEM: nutrient mixture F12 (Ham's) (1:1) (Biological Industries, Israel) at different concentrations. The negative control was prepared as medium without hybrid molecules and treated in the same manner. 100 μ L of medium with or without hybrid molecules were added to each well in triplicate. Following incubation for 24 h at 37 °C, cell viability was evaluated using the 2,3-bis(2-methoxy-4-nitro-5-sulfophenyl)-2H-tetrazolium-5-carboxamide (XTT) cell proliferation assay kit (Biological Industries, Israel) according to the manufacturer's instructions. Briefly, 100 μ L of activation reagent was added to 5 mL of XTT reagent, followed by the addition of 50 μ L of activated-XTT solution to each well. After 2 h incubation at 37 °C, color intensity was measured using an ELISA microplate reader at 450 nm and 630 nm. Results are presented as mean and mean standard error. Each experiment was repeated minimum three times.

Statistics and reproducibility. ThT-binding assays and CD spectrophotometric assays presented in this work were performed at least five times, each time with a minimum of three replicates per condition. Between 8 and 10 representative TEM micrographs and Congo red stained images were acquired at the end of each ThT-binding assay, both for aggregation inhibition and aggregate disruption experiments. XTT viability assays were repeated five times, each time with triplicates for each molecule and concentration.

For the quantitative data derived from ThT and XTT assays, statistical significance, expressed as *p*-value, was determined using Student's *t*-test calculation applied at the end of the experiments, setting tails to 2 (tailed distribution) and type to 2 (samples equal variance), according to reported methods¹²¹. From the XTT viability assays, EC₅₀ and E_{max} values were determined from the dose-response curves of each tested molecule using non-linear least-square data fitting, according to literature¹²².

Reporting summary. Further information on research design is available in the Nature Research Reporting Summary linked to this article.

Data availability

The data associated with the figures presented on this article are available as excel files in the Supplementary Data. Further details generated and analyzed during the current study are available from the corresponding authors upon reasonable request.

Received: 25 February 2020; Accepted: 31 July 2020;

Published online: 02 September 2020

References

- Bayer, T. A. Proteinopathies, a core concept for understanding and ultimately treating degenerative disorders? *Eur. Neuropsychopharmacol.* **25**, 713–724 (2015).
- Chiti, F. & Dobson, C. M. Protein misfolding, functional amyloid, and human disease. *Annu. Rev. Biochem.* **75**, 333–366 (2006).
- Dobson, C. M. Principles of protein folding, misfolding and aggregation. *Semin. Cell Dev. Biol.* **15**, 3–16 (2004).
- Knowles, T. P. et al. Role of intermolecular forces in defining material properties of protein nanofibrils. *Science* **318**, 1900–1903 (2007).
- Mahmoudinobar, F., Urban, J. M., Su, Z., Nilsson, B. L. & Dias, C. L. Thermodynamic stability of polar and nonpolar amyloid fibrils. *J. Chem. Theory Comput.* **15**, 3868–3874 (2019).
- Knowles, T. P. J., Vendruscolo, M. & Dobson, C. M. The amyloid state and its association with protein misfolding diseases. *Nat. Rev. Mol. Cell Biol.* **15**, 384–396 (2014).
- Morel, B., Varela, L. & Conejero-Lara, F. The thermodynamic stability of amyloid fibrils studied by differential scanning calorimetry. *J. Phys. Chem. B* **114**, 4010–4019 (2010).
- Ponjoan, A. et al. Epidemiology of dementia: prevalence and incidence estimates using validated electronic health records from primary care. *Clin. Epidemiol.* **11**, 217–228 (2019).
- Scheltens, P. et al. Alzheimer's disease. *Lancet* **388**, 505–517 (2016).
- Thal, D. R. & Fändrich, M. Protein aggregation in Alzheimer's disease: A β and τ and their potential roles in the pathogenesis of AD. *Acta Neuropathologica* **129**, 163–165 (2015).
- Westermarck, P., Andersson, A. & Westermarck, G. T. Islet amyloid polypeptide, islet amyloid, and diabetes mellitus. *Physiol. Rev.* **91**, 795–826 (2011).
- Haataja, L., Gurlo, T., Huang, C. J. & Butler, P. C. Islet amyloid in type 2 diabetes, and the toxic oligomer hypothesis. *Endocr. Rev.* **29**, 303–316 (2008).
- Westermarck, P. et al. Amyloid fibrils in human insulinoma and islets of Langerhans of the diabetic cat are derived from a neuropeptide-like protein also present in normal islet cells. *Proc. Natl Acad. Sci. U.S.A.* **84**, 3881–3885 (1987).
- Hull, R. L., Westermarck, G. T., Westermarck, P. & Kahn, S. E. Islet amyloid: a critical entity in the pathogenesis of type 2 diabetes. *J. Clin. Endocrinol. Metab.* **89**, 3629–3643 (2004).
- Mulder, H., Gebre-Medhin, S., Betsholtz, C., Sundler, F. & Åhrén, B. Islet amyloid polypeptide (amylin)-deficient mice develop a more severe form of alloxan-induced diabetes. *Am. J. Physiol. Endocrinol. Metab.* **278**, E684–E691 (2000).
- Barbagallo, M. & Dominguez, L. J. Type 2 diabetes mellitus and Alzheimer's disease. *World J. Diabetes* **5**, 889–893 (2014).
- Pruzin, J. J., Nelson, P. T., Abner, E. L. & Arvanitakis, Z. Review: relationship of type 2 diabetes to human brain pathology. *Neuropathol. Appl. Neurobiol.* **44**, 347–362 (2018).
- Macaulay, S. L. et al. Hyperglycemia modulates extracellular amyloid- β concentrations and neuronal activity in vivo. *J. Clin. Invest.* **125**, 2463–2467 (2015).
- Cunnane, S. et al. Brain fuel metabolism, aging, and Alzheimer's disease. *Nutrition* **27**, 3–20 (2011).
- Kim, D. J., Yu, J. H., Shin, M. S., Shin, Y. W. & Kim, M. S. Hyperglycemia reduces efficiency of brain networks in subjects with type 2 diabetes. *PLoS ONE* **11**, e0157268 (2016).
- Rom, S. et al. Hyperglycemia-driven neuroinflammation compromises BBB leading to memory loss in both diabetes mellitus (DM) type 1 and type 2 mouse models. *Mol. Neurobiol.* **56**, 1883–1896 (2019).
- Silzer, T. K. & Phillips, N. R. Etiology of type 2 diabetes and Alzheimer's disease: exploring the mitochondria. *Mitochondrion* **43**, 16–24 (2018).
- Tönnies, E. & Trushina, E. Oxidative stress, synaptic dysfunction, and Alzheimer's disease. *J. Alzheimer's Dis.* **57**, 1105–1121 (2017).
- Irvine, G. B., El-Agnaf, O. M., Shankar, G. M. & Walsh, D. M. Protein aggregation in the brain: the molecular basis for Alzheimer's and Parkinson's diseases. *Mol. Med.* **14**, 451–464 (2008).
- Mukherjee, A. et al. Induction of IAPP amyloid deposition and associated diabetic abnormalities by a prion-like mechanism. *J. Exp. Med.* **214**, 2591–2610 (2017).
- Tjernberg, L. O. et al. A molecular model of Alzheimer amyloid β -peptide fibril formation. *J. Biol. Chem.* **274**, 12619–12625 (1999).
- Scrocchi, L. A. et al. Identification of minimal peptide sequences in the (8–20) domain of human islet amyloid polypeptide involved in fibrillogenesis. *J. Struct. Biol.* **141**, 218–227 (2003).
- Tartaglia, G. G., Cavalli, A., Pellarin, R. & Cafisch, A. Prediction of aggregation rate and aggregation-prone segments in polypeptide sequences. *Protein Sci.* **14**, 2723–2734 (2005).
- Makwana, K. M. & Mahalakshmi, R. Implications of aromatic-aromatic interactions: From protein structures to peptide models. *Protein Sci.* **24**, 1920–1933 (2015).
- Tracz, S. M., Abedini, A., Driscoll, M. & Raleigh, D. P. Role of aromatic interactions in amyloid formation by peptides derived from human Amylin. *Biochemistry* **43**, 15901–15908 (2004).
- Gazit, E. A possible role for π -stacking in the self-assembly of amyloid fibrils. *FASEB J.* **16**, 77–83 (2002).
- Gazit, E. Mechanisms of amyloid fibril self-assembly and inhibition: model short peptides as a key research tool. *FEBS J.* **272**, 5971–5978 (2005).
- Paul, A., Kalita, S., Kalita, S., Sukumar, P. & Mandal, B. Disaggregation of amylin aggregate by novel conformationally restricted aminobenzoic acid containing α/β and α/γ hybrid peptidomimetics. *Sci. Rep.* **7**, 40095 (2017).
- Chemerovski-Glikman, M. et al. Inhibition of the aggregation and toxicity of the minimal amyloidogenic fragment of tau by its pro-substituted analogues. *Chem. - A Eur. J.* **23**, 9618–9624 (2017).
- Zheng, J. et al. Macrocyclic beta-sheet peptides that inhibit the aggregation of a tau-protein-derived hexapeptide. *J. Am. Chem. Soc.* **133**, 3144–3157 (2011).
- Paul, A., Nadimpally, K. C., Mondal, T., Thalluri, K. & Mandal, B. Inhibition of Alzheimer's amyloid- β peptide aggregation and its disruption by a conformationally restricted α/β hybrid peptide. *Chem. Commun.* **51**, 2245–2248 (2015).
- Brahmachari, S., Paul, A., Segal, D. & Gazit, E. Inhibition of amyloid oligomerization into different supramolecular architectures by small

- molecules: mechanistic insights and design rules. *Future Med. Chem.* **9**, 797–810 (2017).
38. Porat, Y., Mazor, Y., Efrat, S. & Gazit, E. Inhibition of islet amyloid polypeptide fibril formation: a potential role for heteroaromatic interactions. *Biochemistry* **43**, 14454–14462 (2004).
39. Franko, A. et al. Epigallocatechin gallate (EGCG) reduces the intensity of pancreatic amyloid fibrils in human islet amyloid polypeptide (hIAPP) transgenic mice. *Sci. Rep.* **8**, 1116 (2018).
40. Du, W.-J. et al. Brazilin inhibits amyloid β -protein fibrillogenesis, remodels amyloid fibrils and reduces amyloid cytotoxicity. *Sci. Rep.* **5**, 7992 (2015).
41. Ehrnhoefer, D. E. et al. EGCG redirects amyloidogenic polypeptides into unstructured, off-pathway oligomers. *Nat. Struct. Mol. Biol.* **15**, 558–566 (2008).
42. KrishnaKumar, V. G., Paul, A., Gazit, E. & Segal, D. Mechanistic insights into remodeled Tau-derived PHF6 peptide fibrils by naphthoquinone-tryptophan hybrids. *Sci. Rep.* **8**, 71 (2018).
43. Paul, A. et al. Novel mannitol-based small molecules for inhibiting aggregation of α -synuclein amyloids in Parkinson's disease. *Front. Mol. Biosci.* **6**, 16 (2019).
44. Paul, A. et al. Antagonistic activity of naphthoquinone-based hybrids toward amyloids associated with Alzheimer's disease and type-2 diabetes. *ACS Chem. Neurosci.* **10**, 3510–3520 (2019).
45. Viswanathan, G. K., Paul, A., Gazit, E. & Segal, D. Naphthoquinone tryptophan hybrids: a promising small molecule scaffold for mitigating aggregation of amyloidogenic proteins and peptides. *Front. Cell Dev. Biol.* **7**, 242 (2019).
46. Scherzer-Attali, R., Shaltiel-Karyo, R., Adalist, Y. H., Segal, D. & Gazit, E. Generic inhibition of amyloidogenic proteins by two naphthoquinone-tryptophan hybrid molecules. *Proteins* **80**, 1962–1973 (2012).
47. Chow, S. C. Bioavailability and bioequivalence in drug development. *Wiley Interdiscip. Rev. Comput. Stat.* **6**, 304–312 (2014).
48. Savjani, K. T., Gajjar, A. K. & Savjani, J. K. Drug solubility: importance and enhancement techniques. *ISRN Pharm.* **2012**, 1–10 (2012).
49. Ruan, H., Sun, Q., Zhang, W., Liu, Y. & Lai, L. Targeting intrinsically disordered proteins at the edge of chaos. *Drug Discov. Today* **24**, 217–227 (2019).
50. Moradi, S. V., Hussein, W. M., Varamini, P., Simerska, P. & Toth, I. Glycosylation, an effective synthetic strategy to improve the bioavailability of therapeutic peptides. *Chem. Sci.* **7**, 2492–2500 (2016).
51. Herter, S. et al. Glycoengineering of therapeutic antibodies enhances monocyte/macrophage-mediated phagocytosis and cytotoxicity. *J. Immunol.* **192**, 2252–2260 (2014).
52. Frenkel-Pinter, M. et al. Selective inhibition of aggregation and toxicity of a tau-derived peptide using its glycosylated analogues. *Chem. - A Eur. J.* **22**, 5945–5952 (2016).
53. Losev, Y. et al. Novel model of secreted human tau protein reveals the impact of the abnormal N-glycosylation of tau on its aggregation propensity. *Sci. Rep.* **9**, 2254 (2019).
54. Paul, A. et al. Tryptophan–glucosamine conjugates modulate tau-derived PHF6 aggregation at low concentrations. *Chem. Commun.* **55**, 14621–14624 (2019).
55. Pawar, A. P. et al. Prediction of “aggregation-prone” and “aggregation-susceptible” regions in proteins associated with neurodegenerative diseases. *J. Mol. Biol.* **350**, 379–392 (2005).
56. Scherzer-Attali, R. et al. Complete phenotypic recovery of an Alzheimer's disease model by a quinone-tryptophan hybrid aggregation inhibitor. *PLoS One* **5**, e11101 (2010).
57. Hussain, M. R. M., Hassan, M., Shaik, N. A. & Iqbal, Z. The role of galactose in human health and disease. *Cent. Eur. J. Med.* **7**, 409–419 (2012).
58. Petry, K. G. & Reichardt, J. K. The fundamental importance of human galactose metabolism: lessons from genetics and biochemistry. *Trends Genet.* **14**, 98–102 (1998).
59. Bartolini, M. et al. Kinetic characterization of amyloid-beta 1–42 aggregation with a multimethodological approach. *Anal. Biochem.* **414**, 215–225 (2011).
60. Scheidt, T. et al. Secondary nucleation and elongation occur at different sites on Alzheimer's amyloid- β aggregates. *Sci. Adv.* **5**, eaau3112 (2019).
61. Wang, S. S., Chen, Y. T. & Chou, S. W. Inhibition of amyloid fibril formation of β -amyloid peptides via the amphiphilic surfactants. *Biochim. Biophys. Acta—Mol. Basis Dis.* **1741**, 307–313 (2005).
62. Greenfield, N. J. Using circular dichroism spectra to estimate protein secondary structure. *Nat. Protoc.* **1**, 2876–2890 (2007).
63. Harada, T. & Kuroda, R. CD measurements of β -amyloid (1–40) and (1–42) in the condensed phase. *Biopolymers* **95**, 127–134 (2011).
64. Vadukul, D. M., Gbajumo, O., Marshall, K. E. & Serpell, L. C. Amyloidogenicity and toxicity of the reverse and scrambled variants of amyloid- β 1–42. *FEBS Lett.* **591**, 822–830 (2017).
65. Paul, A. et al. A peptide based pro-drug disrupts Alzheimer's amyloid into non-toxic species and reduces $\alpha\beta$ induced toxicity in vitro. *Int. J. Pept. Res. Ther.* **24**, 201–211 (2018).
66. Nadimpally, K. C., Paul, A. & Mandal, B. Reversal of aggregation using β -breaker dipeptide containing peptides: Application to A β (1–40) self-assembly and its inhibition. *ACS Chem. Neurosci.* **5**, 400–408 (2014).
67. Wu, C. & Shea, J. E. Structural similarities and differences between amyloidogenic and non-amyloidogenic islet amyloid polypeptide (IAPP) sequences and implications for the dual physiological and pathological activities of these peptides. *PLoS Comput. Biol.* **9**, e1003211 (2013).
68. Krampert, M. et al. Amyloidogenicity of recombinant human pro-islet amyloid polypeptide (ProIAPP). *Chem. Biol.* **7**, 855–871 (2000).
69. Gras, S. L., Waddington, L. J. & Goldie, K. N. Transmission electron microscopy of amyloid fibrils. *Methods Mol. Biol.* **752**, 197–214 (2011).
70. Yakupova, E. I., Bobyleva, L. G., Vikhlyantsev, I. M. & Bobylev, A. G. Congo Red and amyloids: history and relationship. *Biosci. Rep.* **39**, BSR20181415 (2019).
71. Westermark, G. T., Johnson, K. H. & Westermark, P. Staining methods for identification of amyloid in tissue. *Methods Enzymol.* **309**, 3–25 (1999).
72. Tiiman, A., Krishtal, J., Palumaa, P. & Tõugu, V. In vitro fibrillization of Alzheimer's amyloid- β peptide (1–42). *AIP Adv.* **5**, 092401 (2015).
73. Stroud, J. C., Liu, C., Teng, P. K. & Eisenberg, D. Toxic fibrillar oligomers of amyloid- β have cross- β structure. *Proc. Natl Acad. Sci. U.S.A.* **109**, 7717–7722 (2012).
74. Howie, A. J., Brewer, D. B., Howell, D. & Jones, A. P. Physical basis of colors seen in Congo red-stained amyloid in polarized light. *Lab. Invest.* **88**, 232–242 (2008).
75. Bharadwaj, P. R., Dubey, A. K., Masters, C. L., Martins, R. N. & Macreadie, I. G. A β aggregation and possible implications in Alzheimer's disease pathogenesis. *J. Cell. Mol. Med.* **13**, 412–421 (2009).
76. Aguzzi, A. & O'Connor, T. Protein aggregation diseases: pathogenicity and therapeutic perspectives. *Nat. Rev. Drug Discov.* **9**, 237–248 (2010).
77. Höppener, J. W. M., Ahrén, B. & Lips, C. J. M. Islet amyloid and type 2 diabetes mellitus. *N. Engl. J. Med.* **343**, 411–419 (2000).
78. Frydman-Marom, A. et al. Orally administrated cinnamon extract reduces β -amyloid oligomerization and corrects cognitive impairment in Alzheimer's disease animal models. *PLoS One* **6**, e16564 (2011).
79. Magzoub, M. & Miranker, A. D. Concentration-dependent transitions govern the subcellular localization of islet amyloid polypeptide. *FASEB J.* **26**, 1228–1238 (2012).
80. Shaham-Niv, S. et al. Formation of apoptosis-inducing amyloid fibrils by tryptophan. *Isr. J. Chem.* **57**, 729–737 (2017).
81. Manzanera, P. et al. Tryptophan-containing dual neuroprotective peptides: prolyl endopeptidase inhibition and caenorhabditis elegans protection from β -amyloid peptide toxicity. *Int. J. Mol. Sci.* **19**, 1491 (2018).
82. Dubey, K. et al. Tyrosine- and tryptophan-coated gold nanoparticles inhibit amyloid aggregation of insulin. *Amino Acids* **47**, 2551–2560 (2015).
83. Paul, A. et al. Novel mannitol-based small molecules for inhibiting aggregation of α -synuclein amyloids in Parkinson's disease. *Front. Mol. Biosci.* **6**, 16 (2019).
84. Zacco, E. et al. Tailored presentation of carbohydrates on a coiled coil-based scaffold for asialoglycoprotein receptor targeting. *ACS Chem. Biol.* **10**, 2065–2072 (2015).
85. Zacco, E. et al. A self-assembling peptide scaffold for the multivalent presentation of antigens. *Biomacromolecules* **16**, 2188–2197 (2015).
86. Jain, A. et al. Recent advances in galactose-engineered nanocarriers for the site-specific delivery of siRNA and anticancer drugs. *Drug Discov. Today* **23**, 960–973 (2018).
87. Wang, Y., Hong, C.-Y. & Pan, C.-Y. Galactose-based amphiphilic block copolymers: synthesis, micellization, and bioapplication. *Biomacromolecules* **14**, 1444–1451 (2013).
88. Feng, L. et al. Construction of efficacious hepatoma-targeted nanomicelles non-covalently functionalized with galactose for drug delivery. *Polym. Chem.* **5**, 7121–7130 (2014).
89. Demirel, S. et al. Updates on the clinical trials in diabetic macular edema. *Middle East Afr. J. Ophthalmol.* **23**, 3–12 (2016).
90. Cardoso, M. R. D. et al. Adjuvant and immunostimulatory effects of a D-galactose-binding lectin from *Synadenium carinatum* latex (SCLL) in the mouse model of vaccination against neoplasia. *Vet. Res.* **43**, 76 (2012).
91. Sandahl, T. D., Björklund, J. A. E., Laursen, T. L., Ott, P. & Grønbaek, H. The galactose elimination capacity test may monitor treatment response and disease progression in patients with Wilson Disease. *J. Hepatol.* **68**, S631 (2018).
92. Pardridge, W. M. & Oldendorf, W. H. Kinetics of blood-brain barrier transport of hexoses. *BBA - Biomembr.* **382**, 377–392 (1975).
93. Yuan, S. S., Li, M. L., Chen, J. S., Zhou, L. & Zhou, W. Application of mono- and disaccharides in drug targeting and efficacy. *ChemMedChem* **13**, 764–778 (2018).

94. Ruocco, L. A. et al. Galactosylated dopamine enters into the brain, blocks the mesocorticolimbic system and modulates activity and scanning time in Naples high excitability rats. *Neuroscience* **152**, 234–244 (2008).
95. Fernández, C. et al. Synthesis and biological studies of glycosyl dopamine derivatives as potential antiparkinsonian agents. *Carbohydr. Res.* **327**, 353–365 (2000).
96. Gonzalez, J., Fuchs, C., Betts, J. & van Loon, L. Glucose plus fructose ingestion for post-exercise recovery—greater than the sum of its parts? *Nutrients* **9**, 344 (2017).
97. CABI. *The Glycaemic Index: A Physiological Classification of Dietary Carbohydrate* (CABI, 2006). <https://doi.org/10.1079/9781845930516.0000>
98. Tanaka, M., Collins, S. R., Toyama, B. H. & Weissman, J. S. The physical basis of how prion conformations determine strain phenotypes. *Nature* **442**, 585–589 (2006).
99. Chatani, E. & Yamamoto, N. Recent progress on understanding the mechanisms of amyloid nucleation. *Biophys. Rev.* **10**, 527–534 (2018).
100. Knowles, T. P. J. et al. An analytical solution to the kinetics of breakable filament assembly. *Science* **326**, 1533–1537 (2009).
101. Cohen, S. I. A., Vendruscolo, M., Dobson, C. M. & Knowles, T. P. J. From macroscopic measurements to microscopic mechanisms of protein aggregation. *J. Mol. Biol.* **421**, 160–171 (2012).
102. Meng, X., Munishkina, L. A., Fink, A. L. & Uversky, V. N. Molecular mechanisms underlying the flavonoid-induced inhibition of α -synuclein fibrillation. *Biochemistry* **48**, 8206–8224 (2009).
103. Cukalevski, R. et al. Structural changes in apolipoproteins bound to nanoparticles. *Langmuir* **27**, 14360–14369 (2011).
104. Ladiwala, A. R. A., Dordick, J. S. & Tessier, P. M. Aromatic small molecules remodel toxic soluble oligomers of amyloid β through three independent pathways. *J. Biol. Chem.* **286**, 3209–3218 (2011).
105. Kumar, A. et al. Inhibition of A β 42 peptide aggregation by a binuclear ruthenium(II)-Platinum(II) complex: Potential for multimetal organometallics as anti-amyloid agents. *ACS Chem. Neurosci.* **1**, 691–701 (2010).
106. Abelein, A., Lang, L., Lendel, C., Gräslund, A. & Danielsson, J. Transient small molecule interactions kinetically modulate amyloid β peptide self-assembly. *FEBS Lett.* **586**, 3991–3995 (2012).
107. Spiwok, V. CH/ π interactions in carbohydrate recognition. *Molecules* **22**, 1038 (2017).
108. Nishio, M., Umezawa, Y., Fantini, J., Weiss, M. S. & Chakrabarti, P. CH- π hydrogen bonds in biological macromolecules. *Phys. Chem. Chem. Phys.* **16**, 12648–12683 (2014).
109. Quijcho, F. A., Sack, J. S. & Vyas, N. K. Stabilization of charges on isolated ionic groups sequestered in proteins by polarized peptide units. *Nature* **329**, 561–564 (1987).
110. Habchi, J. et al. Systematic development of small molecules to inhibit specific microscopic steps of A β 42 aggregation in Alzheimer's disease. *Proc. Natl Acad. Sci.* **114**, E200–E208 (2017).
111. Taneja, V., Verma, M. & Vats, A. Toxic species in amyloid disorders: oligomers or mature fibrils. *Ann. Indian Acad. Neurol.* **18**, 138 (2015).
112. Stefani, M. Biochemical and biophysical features of both oligomer/fibril and cell membrane in amyloid cytotoxicity. *FEBS J.* **277**, 4602–4613 (2010).
113. Glabe, C. G. Structural classification of toxic amyloid oligomers. *J. Biol. Chem.* **283**, 29639–29643 (2008).
114. Sakono, M. & Zako, T. Amyloid oligomers: formation and toxicity of A β oligomers. *FEBS J.* **277**, 1348–1358 (2010).
115. Young, L. M., Ashcroft, A. E. & Radford, S. E. Small molecule probes of protein aggregation. *Curr. Opin. Chem. Biol.* **39**, 90–99 (2017).
116. Rochet, J.-C. Novel therapeutic strategies for the treatment of protein-misfolding diseases. *Expert Rev. Mol. Med.* **9**, 1–34 (2007).
117. Liu, J., Yang, B., Ke, J., Li, W. & Suen, W.-C. Antibody-based drugs and approaches against amyloid- β species for Alzheimer's disease immunotherapy. *Drugs Aging* **33**, 685–697 (2016).
118. Hampel, H. et al. Advances in the therapy of Alzheimer's disease: targeting amyloid beta and tau and perspectives for the future. *Expert Rev. Neurotherapeutics* **15**, 83–105 (2014).
119. Wisniewski, T. & Konietzko, U. Amyloid- β immunisation for Alzheimer's disease. *Lancet Neurol.* **7**, 805–811 (2008).
120. Doig, A. J. & Derreumaux, P. Inhibition of protein aggregation and amyloid formation by small molecules. *Curr. Opin. Struct. Biol.* **30**, 50–56 (2015).
121. Millar, N. Biology statistics made simple using Excel. *School Sci. Rev.* **83**, 23–34 (2001).
122. Kemmer, G. & Keller, S. Nonlinear least-squares data fitting in Excel spreadsheets. *Nat. Protoc.* **5**, 267–281 (2010).

Acknowledgements

This research was partially supported by the Alliance Family Trust (to D.S.). E.Z. wishes to acknowledge the Daniel Turnberg Travel Fellowship, 2017–2018 scheme, and A.P. is grateful for a British Council, UK-Israel Science Fellowship, 2018–2019 scheme. During writing and revision, E.Z. has received funding from the MINDED fellowship of the European Union's Horizon 2020 research and innovation program under the Marie Skłodowska-Curie grant agreement No. 754490. Authors thank members of the E.G. and D.S. research groups. Authors are grateful to Prof. Annalisa Pastore for valuable comments on this manuscript.

Author contributions

A.P., E.Z., and D.S. planned and designed the experiments. E.Z. and D.S. developed the original idea. A.P. performed of the reported experiments and data analysis. E.Z., M.F.P., D.E.A., and G.M. performed preliminary in vitro experiments. The manuscript was mainly drafted by A.P. and E.Z. with D.S. and E.G. All authors read and approved the manuscript for publication.

Competing interests

The authors declare no competing interests.

Additional information

Supplementary information is available for this paper at <https://doi.org/10.1038/s42003-020-01216-5>.

Correspondence and requests for materials should be addressed to E.Z. or D.S.

Reprints and permission information is available at <http://www.nature.com/reprints>

Publisher's note Springer Nature remains neutral with regard to jurisdictional claims in published maps and institutional affiliations.



Open Access This article is licensed under a Creative Commons Attribution 4.0 International License, which permits use, sharing, adaptation, distribution and reproduction in any medium or format, as long as you give appropriate credit to the original author(s) and the source, provide a link to the Creative Commons license, and indicate if changes were made. The images or other third party material in this article are included in the article's Creative Commons license, unless indicated otherwise in a credit line to the material. If material is not included in the article's Creative Commons license and your intended use is not permitted by statutory regulation or exceeds the permitted use, you will need to obtain permission directly from the copyright holder. To view a copy of this license, visit <http://creativecommons.org/licenses/by/4.0/>.

© The Author(s) 2020